Inorg. Chem. **2004**, *43*, 5011–5020

Application of a Universal Force Field to Mixed Fe/Mo–S/Se Cubane and Heterocubane Clusters. 2. Substitution of Iron by Molybdenum in $Fe_4(S/Se)_4$ Clusters with Terminal Halide and Thiolate Ligands†

Axel Kern, Christian Näther, and Felix Tuczek*

Institut für Anorganische Chemie, Christian Albrechts Universität Kiel, D-24098 Kiel, Germany

Received December 29, 2003

Infrared and Raman spectra of $Fe_4(S/Se)_4$ clusters with terminal halide ligands and $MoFe_3S_4$ clusters with terminal thiolate and halide ligands are presented and interpreted on the basis of the force fields determined in the accompanying paper. The Raman spectra of halide coordinated $Fe_4(S/Se)_4$ clusters are characterized by the fact that vibrations of the terminal ligands appear with little or vanishing intensity. Infrared and Raman spectra of $MoFe_3S_4$ clusters with terminal thiolates are correlated to those of corresponding Fe_4S_4 systems, which were investigated in part 1 of this study and interpreted with normal coordinate analysis. Band assignments are checked by employing $MoFeS_4$ clusters with terminal halide ligands. Spectra of these systems are in turn compared to those of their Fe_4S_4 counterparts, i.e., Fe–S cubane clusters with chloro, bromo, and iodo ligands. A consistent interpretation of all spectra is presented. General implications of these results are discussed.

I. Introduction

Raman spectroscopy has greatly contributed to the elucidation of geometric, vibrational, and electronic structures of iron−sulfur clusters in proteins.[1] In general, these data have been analyzed by spectral comparison with synthetic analogues. This approach might also be employed to obtain more information on the iron−molybdenum cofactor (FeMoco) of nitrogenase, its electronic structure and reactivity. On that score, it is of interest to collect reference data on related model complexes. In the most simple fashion, these are represented by MFe_3S_4 heterocubanes, although, in the meantime, more realistic models of the FeMoco and the P-cluster have been synthesized.[2] The Raman spectroscopic investigation of heterocubane clusters and the spectroscopic comparison to their all-iron analogues allow one to check the generality of the force field developed for Fe_4S_4 clusters,[3] which in the accompanying paper has been applied to a series of $Fe_4(S/Se)_4(S-R/Se-R)_4$ clusters (**1**−**4**). Moreover, it allows one to determine whether heterometal substitution in Fe_4 cubane clusters eventually leads to a decrease in Raman intensity, which might present an experimental obstacle to obtaining Raman spectroscopic information on such systems.

Of particular relevance to the FeMoco are heterocubanes in which one iron atom of the Fe_4S_4 core is substituted by molybdenum.[4] While the hexacoordination of molybdenum in the FeMoco is well reproduced by these systems, the coordination of the iron atoms is different. In the FeMoco, it is close to a trigonal-pyramidal coordination, with three equatorial sulfides and one axial nitrogen, the latter atom representing the recently discovered center of the FeMoco.[5] The iron coordination in $MoFe_3S_4$ heterocubanes, in contrast, is tetrahedral, with three sulfides and one terminal thiolato S donor atom. In the present study, Raman spectra of

* To whom correspondence should be addressed. E-mail: ftuczek@ac.uni-kiel.de.

† Dedicated to Philipp Gütlich on the occasion of his 70th birthday.

(1) (a) Spiro, T. G.; Czernuszewicz, R. S.; Han, S. *Biological Applications of Raman Spectroscopy*; Spiro, T. G., Ed.; John Wiley & Sons: New York, 1988; Chapter 12. (b) Czernuszewicz, R. S.; Kilpatrick, L. K.; Koch, S. A.; Spiro, T. G. *J. Am. Chem. Soc.* **1994**, *116*, 7134−7141. (c) Kilpatrick, L. K.; Kennedy, M. C.; Beinert, H.; Czernuszewicz, R. S.; Qiu, D.; Spiro, T. G. *J. Am. Chem. Soc.* **1994**, *116*, 4053−4061. (d) Han, S.; Czernuszewicz, R. S.; Kimura, T.; Adams, M. W. W.; Spiro, T. G. *J. Am. Chem. Soc.* **1989**, *111*, 3504−3511. (e) Han, S.; Czernuszewicz, R. S.; Spiro, T. G. *J. Am. Chem. Soc.* **1989**, *111*, 3496−3505. (f) Yachandra, K. V.; Hare, J.; Gewirth, A.; Czernuszewicz, R. S.; Kimura, T.; Holm, R. H.; Spiro, T. G. *J. Am. Chem. Soc.* **1983**, *105*, 6462−6468. (g) Yachandra, K. V.; Hare, J.; Moura, I.; Spiro, T. G. *J. Am. Chem. Soc.* **1983**, *105*, 6455−6461. (h) Backes, G.; Mino, Y.; Loehr, T. M.; Meyer, T. E.; Cusanovich, M. A.; Sweeney, W. V.; Adman, E. T.; Sanders-Loehr, J. *J. Am. Chem. Soc.* **1991**, *113*, 2055−2064. (i) Agar, J. N.; Zheng, L.; Cash, V. L.; Dean, D. R.; Johnson, M. K. *J. Am. Chem. Soc.* **2000**, *122*, 2136−2137.

(2) (a) Zhang, Y.; Holm, R. H. *J. Am. Chem. Soc.* **2003**, *125*, 3910−3920. (b) Zhang, Y.; Zuo, J.-L.; Zhou, H.-C.; Holm, R. H. *J. Am. Chem. Soc.* **2002**, *124*, 14292−14293. (c) Zuo, J.-L.; Zhou, H.-C.; Holm, R. H. *Inorg. Chem.* **2003**, *42*, 4624−4631. (d) Ohki, Y.; Sunada, Y.; Honda, M.; Katada, M.; Tatsumi, K. *J. Am. Chem. Soc.* **2003**, *125*, 4052−4053. (e) Coucouvanis, D.; Han, J.; Moon, N. *J. Am. Chem. Soc.* **2002**, *124*, 216−224. (f) Han, J.; Coucouvanis, D. *Inorg. Chem.* **2002**, *41*, 2738−2746.

(3) Czernuszewicz, R. S.; Macor, K. A.; Johnson, M. K.; Gewirth, A.; Spiro, T. G. *J. Am. Chem. Soc.* **1987**, *109*, 7178−7187.

10.1021/ic030346l CCC: $27.50
Published on Web 07/09/2004

$[MoFe_3S_4(S-CH_2-Ph)_3(Cl_4Cat)(CN)]$ (**11**) and $[MoFe_3S_4(S-Et)_3(Cl_4Cat)(CN)]$ (**12**) are presented. The Mo atom is coordinated by tetrachlorocatecholate (Cl_4cat) and cyanide, respectively, in addition to the three sulfides of the cluster core. The iron atoms are coordinated by benzyl thiolate in **11** and ethyl thiolate in **12**. For compound **11**, a normal coordinate analysis is performed.

To obtain more information on the vibrational properties of $MoFe_3S_4$ clusters and to check the assignments made in the analysis of the $MoFe_3S_4$−benzyl cluster **11**, $MoFe_3S_4$ clusters with terminal chloro and bromo ligands were prepared and investigated with IR and Raman spectroscopy. In the present study, the spectra of $[MoFe_3S_4Cl_3(Cl_4Cat)L]^{2-}$ (**13**) and $[MoFe_3S_4Br_3(Cl_4Cat)L]^{2-}$ (**14**; L = solvent) are presented and analyzed. The spectra of these systems are in turn correlated to those of a series of all-iron $Fe_4(S/Se)_4Hal_4$ clusters with terminal Hal ligands (**5**−**10**; Hal = chloro, bromo, and iodo). Without organic residues, these clusters are smaller than their thiolate/selenolate coordinated counterparts **1**−**4**. Moreover, the Raman spectra are free of innerligand bands. Raman intensities, however, decrease because of a lack of resonance enhancement, as the CT transition at about 420−470 nm, which is characteristic of the analogous thiolate/selenolate coordinate clusters, is lacking.[6] Nevertheless, good quality Raman and IR spectra of a complete series of $Fe_4(S/Se)_4$−halide coordinated cubanes could be obtained, i.e., $(TBA)_2[Fe_4S_4Cl_4]$ (**5**), $(TBA)_2[Fe_4S_4Br_4]$ (**6**), $(TBA)_2[Fe_4S_4I_4]$ (**7**), $(TBA)_2[Fe_4Se_4Cl_4]$ (**8**), $(TBA)_2[Fe_4Se_4Br_4]$ (**9**), and $(TBA)_2[Fe_4Se_4I_4]$ (**10**; TBA = tetra-*n*-butylammonium). These systems were prepared by an established route.[7] For compound **10**, an X-ray crystal structure determination has been performed.

The spectra of the Fe_4S_4 clusters with halide ligands **5**−**10** are presented in the first part of the Results and Analysis section and are evaluated by normal coordinate analysis. The corresponding force fields are derived from those of the corresponding thiolato/selenolato clusters obtained in part 1 of this study. Then, vibrational spectroscopic data of $MoFe_3S_4$ systems with terminal thiolate and halide ligands are presented and analyzed. On the basis of the information collected from the study of its Fe_4S_4 analogue, the spectrum of the $MoFe_3S_4$−benzyl cluster **11** is interpreted, and a normal coordinate analysis is performed. The corresponding band assignments are checked by an analysis of the spectra of $MoFe_3S_4$ clusters with terminal halide ligands, i.e., **13** and **14**. Finally, the spectroscopic results obtained in this study are summarized, and their general implications are discussed.

Table 1. Crystal Data and Results of the Structure Refinement for Compound **10**[a]

chemical formula	$[Fe_4Se_4I_4](C_{16}H_{36}N)_2$
fw	1531.76
T	150 K
λ	0.710 73 Å
cryst syst	orthorhombic
space group	$P2_1/n$
a	12.201(1) Å
b	23.093(2) Å
c	18.176(1) Å
γ	90.74(1)°
V	5120.9(6) Å^3
Z	4
D_{calcd}	1.987 g cm^{-3}
μ	6.42 cm^{-1}
R_1 [$I > 2\sigma(I)$]	0.0258
wR_2 [all data]	0.0681

[a] $R_1 = \sum||F_o| - |F_c||/\sum|F_o|$; $wR_2 = [\sum[w(F_o^2 - F_c^2)^2]/\sum[w(F_o^2)^2]]$.

II. Experimental Section

All reactions were performed using Schlenk techniques on a vacuum/inert gas line (Argon 4.6). Compounds were handled and samples for spectroscopy were prepared in gloveboxes (M. Braun, Labmaster 130) in an argon atmosphere.

Preparation of $Fe_4(S/Se)_4$−Halide Clusters. $[Fe_4(S/Se)_4X_4]^{2-}$ clusters (X = Cl, Br, or I) were prepared as tetrabutylammonium salts (TBA) following published methods.[7] TBA salts of $[Fe_4(S/Se)_4(SR)_4]^{2-}$ clusters with different thiolate residues were used as precursors. The published procedure was slightly modified as will be outlined.

TBA−$[Fe_4S_4Cl_4]$ (5). TBA−$[Fe_4S_4(S-{}^iPr)_4]$ was reacted in acetonitrile with benzoyl chloride in a ratio of 1:12. After a reaction time of 1 h, a 3-fold volume of diethyl ether was added, and the mixture was cooled to −40 °C to precipitate the product. The compound was recrystallized from acetonitrile/isopropyl alcohol.

TBA−$[Fe_4S_4Br_4]$ (6). TBA−$[Fe_4S_4(S-CH_2-C_6H_4-Cl^{para})_4]$ (4.2 g, 2.85 mmol) was slurried in 65 mL acetonitrile, and after 1 h of stirring, the volume of the reaction mixture was reduced in vacuo to 30 mL. Then, 60 mL of diethyl ether and 20 mL of THF were added, and the solution was cooled to −40 °C. The product was obtained as thin black crystals which were collected by filtration, washed with diethyl ether, and dried in vacuo. The compound was used without further recrystallization.

TBA−$[Fe_4S_4I_4]$ (7). This compound was prepared by exchange of the chloro ligands of **5** with iodide. The ratio of TBA−$[Fe_4S_4Cl_4]$ to sodium iodide was 1:11. The compound was recrystallized from acetonitrile/diethyl ether.

TBA−$[Fe_4Se_4Cl_4]$ (8). This compound was prepared analogously to **5** and **6**. The ratio of TBA−$[Fe_4Se_4(S-CH_2-C_6H_4)_4]$ to benzoyl chloride was 1:12. After addition of diethyl ether, the solution was cooled to −40 °C. The isolated compound was recrystallized from acetonitrile/isopropyl alcohol.

(4) (a) Palermo, R. E.; Holm, R. H. *J. Am. Chem. Soc.* **1983**, *105*, 4310−4318. (b) Palermo, R. E.; Singh, R.; Bashkin, J. K.; Holm, R. H. *J. Am. Chem. Soc.* **1984**, *106*, 2600−2612. (c) Wolff, T. E.; Berg, J. M.; Holm, R. H. *Inorg. Chem.* **1981**, *20*, 174−180. (d) Huang, J.; Goh, C.; Holm, R. H. *Inorg. Chem.* **1997**, *36*, 356−361. (e) Osterloh, F.; Segal, B. M.; Achim, C.; Holm, R. H. *Inorg. Chem.* **2000**, *39*, 980−989. (f) Zhang, Y.-P.; Bashkin, J. K.; Holm, R. H. *Inorg. Chem.* **1987**, *26*, 694−702. (g) Demadis, K. D.; Coucouvanis, D. *Inorg. Chem.* **1995**, *34*, 436−448. (h) Holm, R. H.; Simhon, E. D. In *Molybdenum Enzymes*; Spiro, T. G., Ed.; John Wiley & Sons: New York, 1985; pp 1−88. (i) Demadis, K. D.; Malinak, S. M.; Coucouvanis, D. *Inorg. Chem.* **1996**, *35*, 4038−4046. (j) Fomitchev, D. V.; McLauchlan, C. C.; Holm, R. H. *Inorg. Chem.* **2002**, *41*, 958−966. (k) Laughlin, L. J.; Coucouvanis, D. *J. Am. Chem. Soc.* **1996**, *118*, 3118−3125. (l) Demadis, K. D.; Coucouvanis, D. *Inorg. Chem.* **1995**, *34*, 3658−3666. (m) Coucouvanis, D. *Acc. Chem. Res.* **1991**, *24*, 1. (n) Coucouvanis, D. In *Molybdenum Enzymes, Cofactors and Model Systems*; Stiefel, E. I., Coucouvanis, D., Newton, W. E., Eds.; American Chemical Society: Washington, DC, 1993; pp 304−331.

(5) Einsle, O.; Tezcan, F. A.; Andrade, S. L. A.; Schmid, B.; Yoshida, M.; Howard, J. B.; Rees, D. C. *Science* **2002**, *297*, 1696−1700 and references cited therein.

(6) (a) Aizman, A.; Case, D. A. *J. Am. Chem. Soc.* **1982**, *104*, 3269−3279. (b) Noodleman, L.; Norman, J. G.; Osborne, J. H.; Aizman, A.; Case, D. A. *J. Am. Chem. Soc.* **1985**, *107*, 3418−3426.

(7) Wong, G. B.; Bobrick, M. A.; Holm, R. H. *Inorg. Chem.* **1978**, *17*, 578−584.

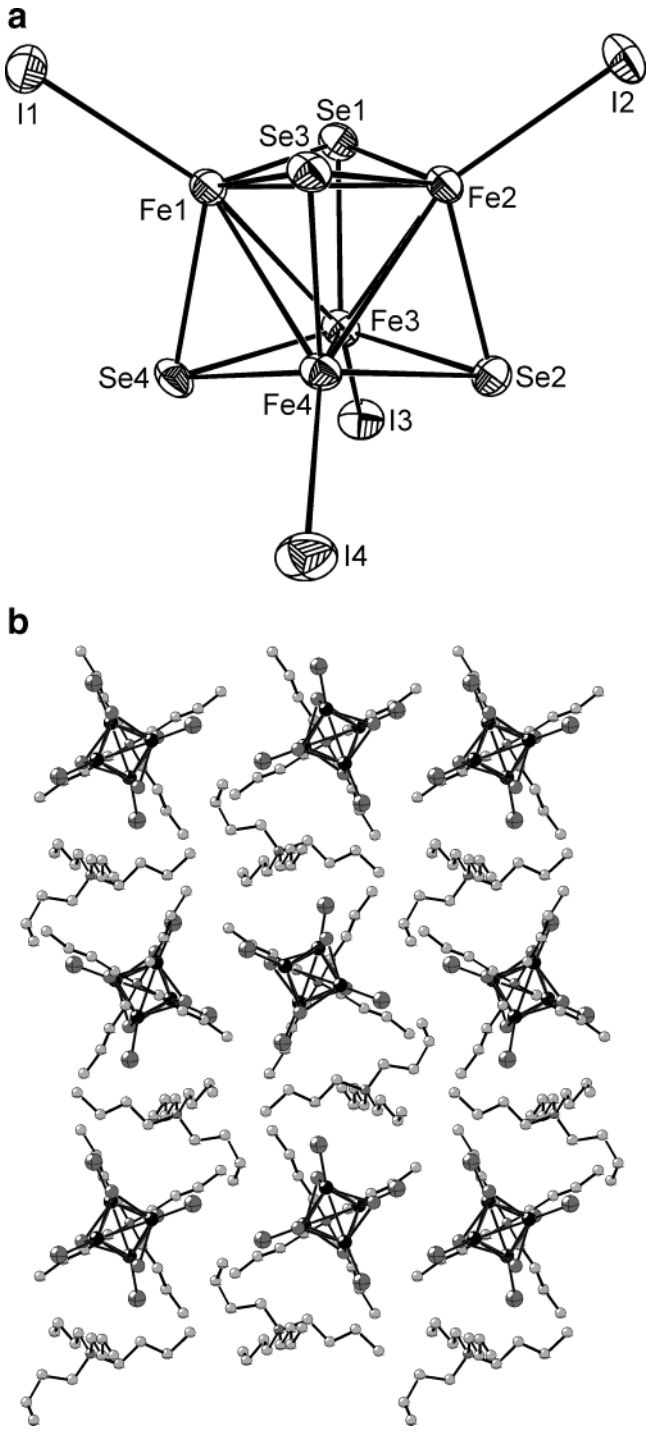

Figure 1. a. Crystal structure of the $[Fe_4Se_4I_4]$ unit of compound **10** with labeling and displacement ellipsoids drawn at the 50% probability level. b. Crystal structure of compound **10** with view along the crystallographic *a*-axis (hydrogen atoms are omitted for clarity).

TBA−[$Fe_4Se_4Br_4$] (9). TBA−$[Fe_4Se_4(S-CH_2-C_6H_4-OCH_3^{para})_4]$ was reacted with benzoyl bromide for 1.5 h. Precipitation of the product was caused by adding a 1.5-fold volume of diethyl ether and cooling to −40 °C. The compound was recrystallized from acetonitrile/diethyl ether.

TBA−[$Fe_4Se_4I_4$] (10). TBA−$[Fe_4Se_4Cl_4]$ (**8**) (0.35 g, 0.3 mmol) was dissolved in 20 mL of acetonitrile. A solution of 0.36 g (2.4 mmol) of NaI in 10 mL of acetonitrile was added, and the reaction mixture was stirred for 1 h, filtered, and cooled to −40 °C. The precipitated black material was filtered off, washed with isopropyl alcohol, and dried in vacuo. After further cooling of the filtrate, rodlike black crystals were obtained, which were collected by filtration and washed with isopropyl alcohol.

Table 2. Selected Distances (Å) and Angles (deg) for Compound **10**

Fe(1)−Se(4)	2.3872(5)	Fe(1)−Se(3)	2.3982(6)
Fe(1)−Se(1)	2.4084(6)	Fe(1)−I(1)	2.5653(6)
Fe(1)−Fe(3)	2.8104(7)	Fe(1)−Fe(4)	2.8116(7)
Fe(1)−Fe(2)	2.8248(7)	Fe(2)−Se(2)	2.3786(6)
Fe(2)−Se(3)	2.4017(6)	Fe(2)−Se(1)	2.4103(6)
Fe(2)−I(2)	2.5502(5)	Fe(2)−Fe(3)	2.7790(6)
Fe(2)−Fe(4)	2.7849(7)	Fe(3)−Se(2)	2.4023(6)
Fe(3)−Se(1)	2.4025(6)	Fe(3)−Se(4)	2.4043(6)
Fe(3)−I(3)	2.5570(5)	Fe(3)−Fe(4)	2.7694(7)
Fe(4)−Se(3)	2.3878(5)	Fe(4)−Se(2)	2.3888(6)
Fe(4)−Se(4)	2.4063(6)	Fe(4)−I(4)	2.5410(5)
Se(4)−Fe(1)−Se(3)	105.43(2)	Se(4)−Fe(1)−Se(1)	105.58(2)
Se(3)−Fe(1)−Se(1)	105.47(2)	Se(2)−Fe(2)−Se(3)	105.74(2)
Se(2)−Fe(2)−Se(1)	106.69(2)	Se(3)−Fe(2)−Se(1)	105.31(2)
Se(2)−Fe(3)−Se(1)	106.18(2)	Se(2)−Fe(3)−Se(4)	106.80(2)
Se(1)−Fe(3)−Se(4)	105.23(2)	Se(3)−Fe(4)−Se(2)	105.86(2)
Se(3)−Fe(4)−Se(4)	105.16(2)	Se(2)−Fe(4)−Se(4)	107.17(2)
Se(4)−Fe(1)−I(1)	112.63(2)	Se(3)−Fe(1)−I(1)	109.92(2)
Se(1)−Fe(1)−I(1)	116.96(2)	Se(1)−Fe(2)−I(2)	112.44(2)
Se(2)−Fe(2)−I(2)	111.32(2)	Se(3)−Fe(2)−I(2)	114.75(2)
Se(2)−Fe(3)−I(3)	109.04(2)	Se(1)−Fe(3)−I(3)	117.10(2)
Se(4)−Fe(3)−I(3)	111.88(2)	Se(3)−Fe(4)−I(4)	115.72(2)
Se(2)−Fe(4)−I(4)	111.28(2)	Se(4)−Fe(4)−I(4)	111.10(2)
Fe(3)−Fe(1)−Fe(4)	59.02(2)	Fe(3)−Fe(1)−Fe(2)	59.10(2)
Fe(4)−Fe(1)−Fe(2)	59.22(2)	Fe(3)−Fe(2)−Fe(1)	60.20(2)
Fe(4)−Fe(2)−Fe(1)	60.15(2)	Fe(3)−Fe(2)−Fe(4)	59.70(2)
Fe(4)−Fe(3)−Fe(2)	60.26(2)	Fe(2)−Fe(3)−Fe(1)	60.71(2)
Fe(4)−Fe(3)−Fe(1)	60.51(2)	Fe(3)−Fe(4)−Fe(2)	60.04(2)
Fe(3)−Fe(4)−Fe(1)	60.47(2)	Fe(2)−Fe(4)−Fe(1)	60.63(2)
Fe(3)−Se(1)−Fe(1)	71.49(2)	Fe(3)−Se(1)−Fe(2)	70.54(2)
Fe(1)−Se(1)−Fe(2)	71.78(2)	Fe(2)−Se(2)−Fe(4)	71.49(2)
Fe(2)−Se(2)−Fe(3)	71.08(2)	Fe(4)−Se(2)−Fe(3)	70.62(2)
Fe(4)−Se(3)−e(1)	71.95(2)	Fe(4)−Se(3)−Fe(2)	71.11(2)
Fe(1)−Se(3)−Fe(2)	72.10(2)	Fe(1)−Se(4)−Fe(3)	71.82(2)
Fe(1)−Se(4)−Fe(4)	71.82(2)	Fe(3)−Se(4)−Fe(4)	70.30(2)

$(Et_4N)_3[MoFe_3S_4(S-CH_2-C_6H_4)_3(Cl_4cat)(CN)]$ (11). $(Et_4N)_3[MoFe_3S_4(S-C_2H_5)_3(Cl_4cat)(CN)]$ (**12**)[4b] (0.37 g, 0.3 mmol) was dissolved in 120 mL of acetonitrile, and 0.21 mL (1.6 mmol) of benzyl mercaptane was added. The reaction mixture was stirred for 4 h and placed under vacuum every 20 min to remove the ethanethiol which was liberated in the substitution reaction. After stirring overnight, the solution was reduced in vacuo to 40 mL, and, after an additional 3 h of stirring, reduced to 20 mL. At a temperature of 40 °C, the mixture was again evacuated several times. Adding 30 mL of methanol and cooling the solution to −40 °C for several days caused the precipitation of a black product, which was filtered off and dried in vacuo. Compound **12** was prepared after ref 4b.

Preparation of the $MoFe_3S_4$−Halide Clusters. The $[MoFe_3S_4X_3(Cl_4cat)L]^{2-}$ clusters (X = Cl or Br; L = solvent) were prepared following a literature method for a similar compound.[4a]

$(Et_4N)_2[MoFe_3S_4Cl_3(Cl_4cat)L]$ (13). To a solution of 1.08 g (0.5 mmol) of $(Et_4N)_4[Mo_2Fe_6S_8(SEt)_6(Cl_4cat)_2]$[4b] in 160 mL of acetonitrile was added dropwise a solution of 0.25 mL (3.3 mmol) of acetyl chloride in 50 mL of acetonitrile at a temperature of 0 °C. After 1 h of stirring at room temperature, the solvent was removed by evaporation, and the residue was extracted with 50 mL of acetone, filtered, and reduced to 20 mL in vacuo. Addition of 35 mL of THF and cooling for 7 days to −40 °C caused the precipitation of a black solid, which was filtered off, washed with THF (3 × 10 mL), and dried in vacuo.

$(Et_4N)_2[MoFe_3S_4Br_3(Cl_4cat)L]$ (14). The preparation of this compound is analogous to that employed for the preparation of $(Et_4N)_2[MoFe_3S_4Cl_3(Cl_4cat)L]$ (**13**), except for an initial volume of 200 mL (instead of 160 mL) of acetonitrile and addition of 15 mL of acetonitrile (instead of acetone) to the dried residue. Adding

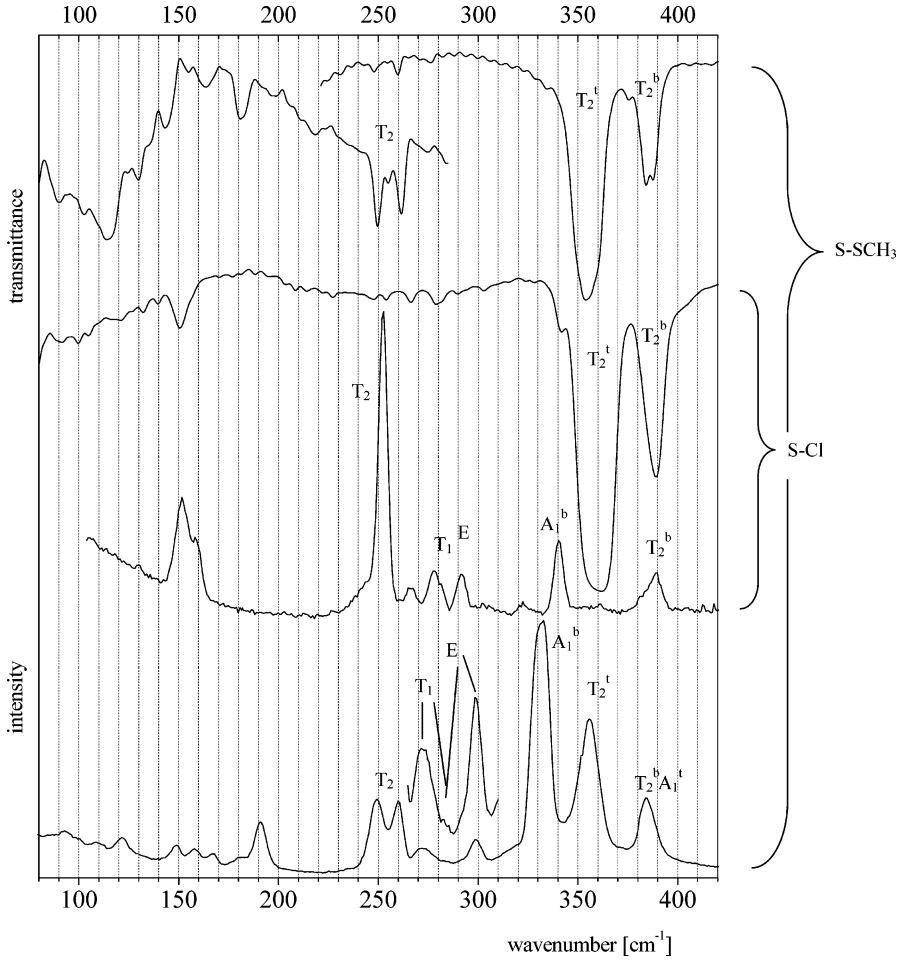

Figure 2. Raman and IR spectra of $[Fe_4S_4(S-CH_3)_4]^{2-}$ and $[Fe_4S_4Cl_4]^{2-}$.

45 mL of toluene to the filtered solution and cooling to −40 °C caused the precipitation of a black solid.

X-ray structure determination of **10** was performed using an STOE IPDS diffractometer and was corrected for absorption effects. The structure was solved with direct methods using SHELXS-97 and was refined against F^2 using SHELXL-97. All non-H atoms were refined anisotropically. The H atoms were positioned with idealized geometry and refined using the riding model. Table 1 gives the crystal data of $(TBA)_2[Fe_4Se_4I_4]$ (**10**).

Raman spectra were recorded on a commercial spectrometer (DILOR XY) equipped with a triple monochromator and a CCD camera (ISA Spectrum One). The excitation source was a 2018 Ar^+/Kr^+ mixed-gas laser from Spectra Physics. All samples were measured as KBr and RbI pellets, respectively, employing laser powers of 15−25 mW and a spectral resolution of 1.5 cm^{-1}. The sample temperature was kept at 20 K. Infrared spectra were recorded on a Bruker IFS 66 FTIR spectrometer equipped with a CTI cryocooler. The temperature of the sample was set at 20 K. Normal coordinate analyses were performed with the program MOLVIB.[8]

III. Results and Analysis

A. X-ray Structure Determination of $(TBA)_2[Fe_4Se_4I_4]$ (10). Structural information on all $[Fe_4(S/Se)_4Hal_4]$ clusters with Hal = Cl, Br, and I is available, with the exception of the $Fe_4Se_4I_4$ cluster (**10**).[9] Therefore, an X-ray crystal structure determination of this system was performed. Compound **10** crystallizes in the monoclinic space group $P2_1/n$ with four formula units in the unit cell. The asymmetric unit consists of $[Fe_4Se_4I_4]^{2-}$ units and two crystallographically independent tetrabutylammonium cations, all of which are located in general positions. In the $[Fe_4Se_4I_4]$ cluster, the iron atoms are tetrahedrally coordinated by selenium and iodine (Figure 1a). Bond distances and angles are given in Table 2. In the crystal structure of **10**, the $[Fe_4Se_4I_4]^{2-}$ unit and one of the crystallographically independent tetrabutylammonium cations form alternating stacks in the direction of the *a*-axis (Figure 1b). These stacks are arranged in layers parallel to the *ac*-plane, which are separated by the second crystallographically independent tetrabutylammonium cations.

B. Spectra of $Fe_4(S/Se)_4Hal_4$ Clusters with Terminal Halide Ligands; Hal = Cl, Br, and I. Infrared and Raman spectra of the Fe_4S_4 clusters with terminal halide ligands, i.e., TBA−$[Fe_4S_4Cl_4]$ (**5**), TBA−$[Fe_4S_4Br_4]$ (**6**), and TBA−

(8) (a) Sundius, T. QCPE No. 604, MOLVIB; Indiana University: Indiana 1991. Modified: Bublitz, D. Ph.D. Dissertation, Universität Kiel, 1995. (b) Sundius, T. *J. Mol. Struct.* **1990**, *218*, 321−326. (c) Sundius, T. *Commentat. Phys.−Math.* **1977**, *47*, 1−66.

(9) Structural data for $Fe_4(S/Se)_4Hal_4$: (a) Bobrick, M. A.; Hodgson, K. O.; Holm, R. H. *Inorg. Chem.* **1977**, *16*, 1851−1858. (b) Müller, A.; Schladerbeck, N. H.; Bogge, H. *Chimia* **1985**, *39*, 24. (c) Müller, A.; Schladerbeck, N. H.; Krickemeyer, E.; Bögge, H.; Schmitz, K.; Bill, E.; Trautwein, A. X. *Z. Anorg. Allg. Chem.* **1989**, *570*, 7−36. (d) Pohl, S.; Saak, W. *Z. Naturforsch., B: Chem. Sci.* **1988**, *43*, 457. (e) Cen, W.; Liu, H. *Jiegou Huaxue* **1986**, *5*, 203. (f) Rutchik, S.; Kim, S.; Walters, M. A. *Inorg. Chem.* **1988**, *27*, 1513−1516.

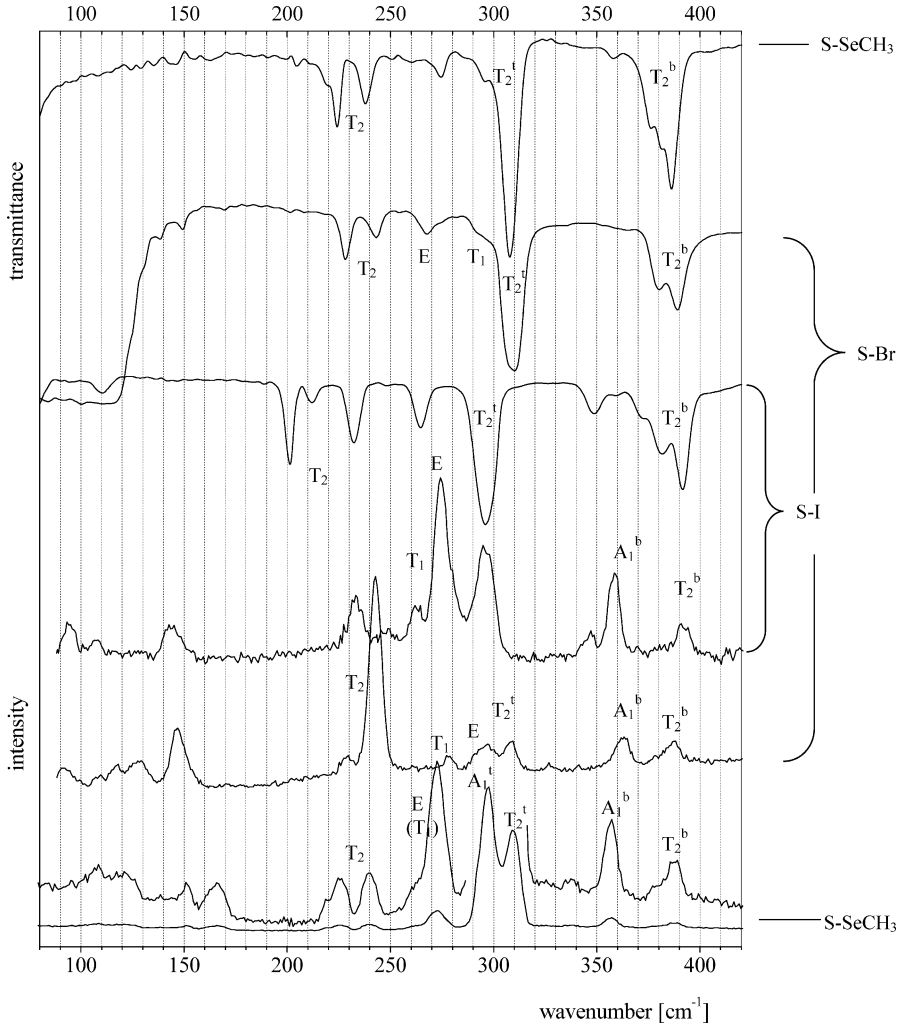

Figure 3. Raman and IR spectra of $[Fe_4S_4(Se-CH_3)_4]^{2-}$ and $[Fe_4S_4Br_4]^{2-}$/$[Fe_4S_4I_4]^{2-}$.

$[Fe_4S_4I_4]$ (**7**), are shown in Figures 2 and 3, along with spectra of corresponding Fe_4S_4 clusters with thiolate and selenolate ligands, i.e., TBA−$[Fe_4S_4(S-CH_3)_4]$ (**1**) and $[Fe_4S_4(Se-CH_3)_4]$ (**3**). Figures 4 and 5 give the spectra of the analogous selenoclusters, i.e., TBA−$[Fe_4Se_4Cl_4]$ (**8**), TBA−$[Fe_4SeBr_4]$ (**9**), and TBA−$[Fe_4Se_4I_4]$ (**10**), which are compared to the spectra of corresponding thiolate and selenolate coordinated selenoclusters, $[Fe_4Se_4(S-CH_3)_4]$ (**2**) and $[Fe_4Se_4(Se-CH_3)_4]$ (**4**), respectively (cf. accompanying paper). As is apparent from these figures, the far-IR segment of the spectra of halide coordinated cubanes **5**−**10** is dominated by two intense bands (partly split) which are assigned to the higher energy terminal (t) and bridging (b) T_2 modes II (T_2^t) and III (T_2^b), respectively (the designation of the modes refers to the accompanying paper). Comparison with the spectra of corresponding $Fe_4(S/Se)^b{}_4(S/Se)^t{}_4$ clusters **1**−**4** clearly demonstrates the relationship between clusters containing terminal ligands of similar mass, sulfur and chlorine on one hand and selenium and bromine on the other hand; i.e., iron-sulfur and -selenoclusters with chloride ligands exhibit the same spectral pattern in the far-IR and Raman spectra as corresponding clusters with thiolate ligands (Figures 2 and 4), and $Fe_4(S/Se)_4$ clusters with bromide ligands exhibit the same spectral pattern as corresponding clusters with selenolate ligands (Figures 3 and 5). For both sulfur clusters and selenoclusters, substitution of bromine by iodine causes a further downshift in energy of the terminal modes by 20−25 cm^{-1} (Figures 3 and 5). The third respective band of T_2 symmetry, VII, appears with variable intensity at lower energy. Assignment of the T_2 bands thus is already achieved on the basis of a comparison of the FTIR spectra (Table 3). Moreover, splitting of these bands provides information with respect to a lowering of the symmetry. Besides E and B_2 modes of T_2 parentage, only the $A_2(T_1)$ mode is IR active in D_{2d} point group symmetry. The presence of additional bands in the FTIR spectra besides these features thus indicates a symmetry reduction below D_{2d}.

Raman spectra of the Fe_4S_4 clusters with terminal halides are characterized by the fact that vibrations of predominantly terminal character like I (A_1^t) and II (T_2^t) are weak or missing altogether. Further band assignments were made primarily on the basis of normal coordinate analysis. For the chloride coordinated clusters, the force fields were derived from the corresponding sulfur clusters and selenoclusters with terminal thiolate ligands, and for the bromide coordinated clusters, the force fields were derived from the corresponding sulfur clusters and selenoclusters with terminal selenolate ligands, which is in agreement with the spectral similarities consid-

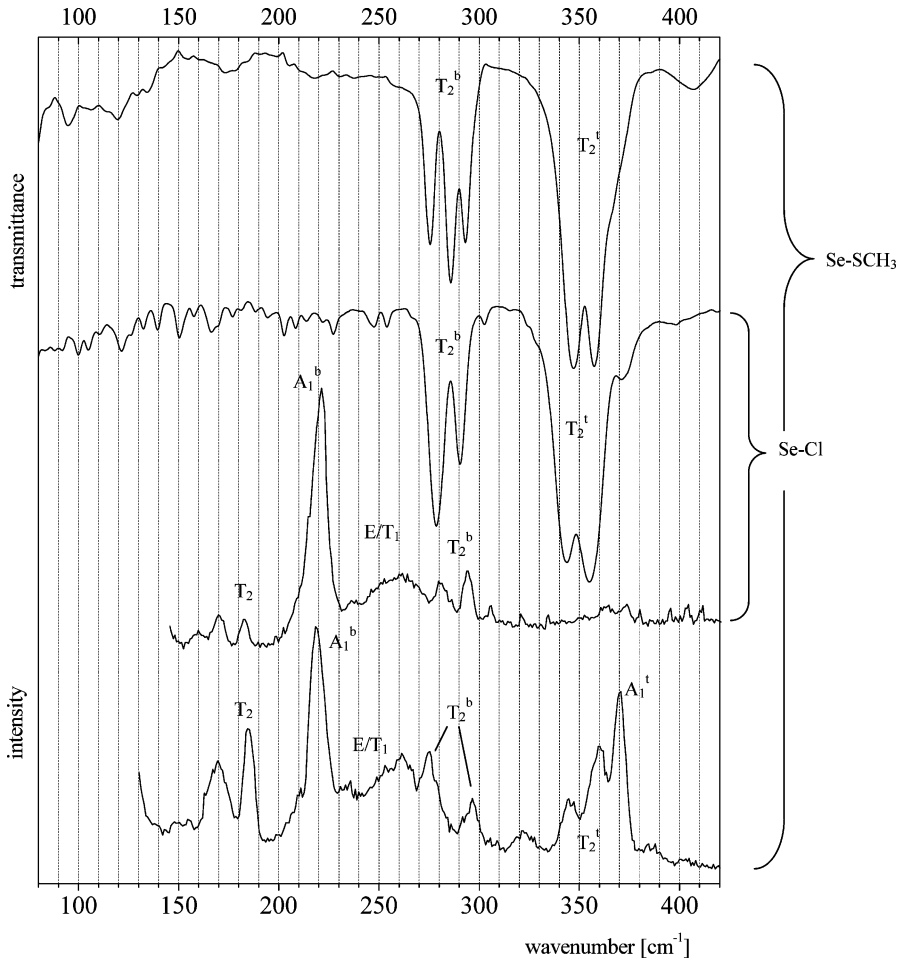

Figure 4. Raman and IR spectra of $[Fe_4Se_4(S-CH_3)_4]^{2-}$ and $[Fe_4Se_4Cl_4]^{2-}$.

ered already. To adjust the parameters of the thiolate and selenolate coordinated clusters to those of the halide coordinated clusters, scaling procedures such as those outlined in the accompanying paper were employed. Structural information was taken from the literature and from the X-ray structure determination of the $Fe_4Se_4I_4$ cluster (**10**), respectively (vide supra). Molecular parameters adjusted to tetrahedral symmetry are collected in Table 4. For the iodo coordinated clusters, the Fe−Hal force constant was varied until agreement with the measured frequencies was achieved.

To obtain overall good agreement between calculated and observed frequencies, it became necessary to introduce small off-diagonal matrix elements *f*'s between bridging coordinates on one hand and between bridging and terminal coordinates on the other hand. Alternate force fields without these force constants *f*'s are given as well but cannot be applied to all clusters. Calculated frequencies are given along with the observed values in Table 3. The corresponding force constants are collected in Table 5.

C. Spectra of $MoFe_3S_4$ Clusters with Terminal Thiolate and Halide Ligands. Raman spectra of $MoFe_3S_4$ clusters were found to exhibit relatively broad bands and comparatively small resonance enhancements. Nevertheless, spectra of sufficient quality could be obtained. The IR and Raman spectra of the $MoFe_3S_4$−benzyl cluster TEA−$[MoFe_3S_4$(S−

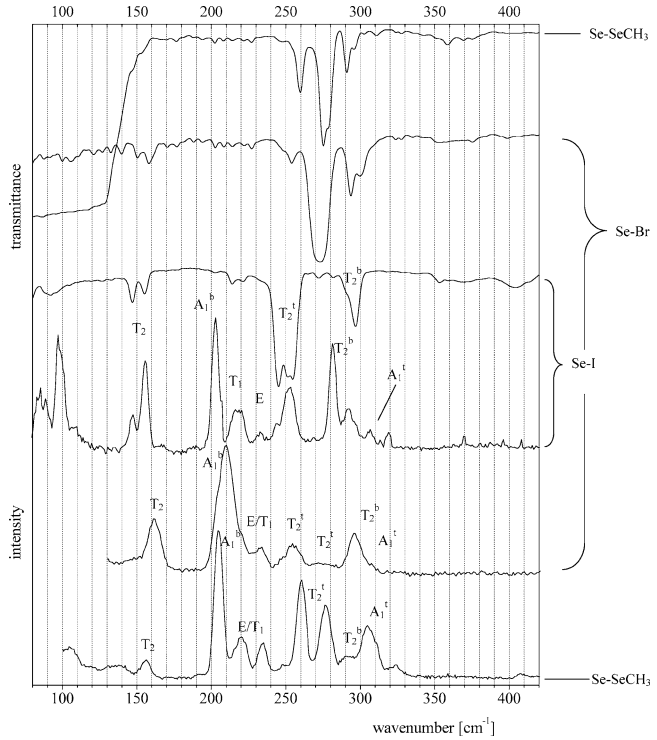

Figure 5. Raman and IR spectra of $[Fe_4Se_4(Se-CH_3)_4]^{2-}$ and $[Fe_4Se_4Br_4]^{2-}$/$[Fe_4Se_4I_4]^{2-}$.

Table 3. Fe_4S_4 Clusters with Halide Ligands in T_d Symmetry: Observed and Calculated Frequencies

A_1^{Fe}	A_1^t I	T_2^t II	T_2^b III	A_1^b IV	E^b V	T_1^b VI	T_2^b VII		*a*
				S−Cl (5)					
152		360	389	341	292	278	253	obsd	
170	404	361	390	338	291	281	259	calcd	b
175	399	361	389	339	292	280	252	calcd	c
153	397	363	385	337	292	283	253	calcd	d
				S−Br (6)					
		310	384	363	292	279	230/242	obsd	
139	326	311	382	363	290	280	237	calcd	
				S−I (7)					
		296	381/391	359	274	264	232	obsd	
112	323	295	384	360	271	264	229	calcd	c
111	330	297	384	362	280	271	231	calcd	d
				Se−I (8)					
86/98	281	245/252	290/296	203	232	214/221	147/155	obsd	
102	306	253	286	203	232	219	150	calcd	
				Se−Br (9)					
		273	293/297/300	210	255	230/233	161	obsd	
127	320	270	298	210	250	234	160	calcd	
				Se−Cl (10)					
	360	344/355	279/293	221	247/254	235	170/183	obsd	
151	363	347	277	218	248	235	179	calcd	

[a] Refers to alternate force fields; corresponding frequencies are given in Table 5.

$CH_2C_6H_5)_3(Cl_4cat)(CN)]$ (**11**) are shown in Figure 6. Frequencies and band assignments are collected in Table 5. On the basis of the vibrational frequencies observed for **11**, the structural model given in Figure 7, and the force field of the Fe_4S_4−benzyl cluster, a normal coordinate analysis was performed. The geometry parameters of the $[MoFe_3S^b_4S^t_3O_3]$ molecular fragment of Figure 7 are adapted from the X-ray structure determination of the ethyl thiolate cluster (**12**)[4b] and averaged to C_{3v} symmetry (cf. Table 7). Moreover, the three terminal metal−ligand bonds on the Mo center are considered as Mo−O bonds, although in reality, only two of these bonds correspond to Mo−O(catecholate), and the third ligand is CN^-. The corresponding molecular unit has 18 stretching modes, which can be divided into 3 Mo−O and 15 Mo/Fe−S vibrations. In C_{3v} symmetry, these transform according to

$$\Gamma^{Mo-O} = A_1 + E \quad (3) \tag{1a}$$

and

$$\Gamma^{Mo/Fe-S} = 4A_1 + A_2 + 5E \quad (15) \tag{1b}$$

specifically

$$\Gamma^{Mo-S} = A_1 + E \quad (3) \tag{2a}$$

$$\Gamma^{Fe-St} = A_1 + E \quad (3) \tag{2b}$$

$$\Gamma^{Fe-Sb} = 2A_1 + A_2 + 3E \quad (9) \tag{2c}$$

The correlation with the vibrations of the $Fe_4S_4X_4$ systems (X = S, Se, Hal) thus is as follows:

$$A_1^t(I) + T_2^t(II) \rightarrow A_1(Mo-O) + E(Mo-O) + A_1(Fe-S^t) + E(Fe-S^t) \tag{3a}$$

(note that there are two more t vibrations in the $MoFe_3S_4$ than in the Fe_4S_4 cluster) and

$$T_2^b(III) + A_1^b(IV) + E^b(V) + T_1^b(VI) + T_2^b(VII) \rightarrow A_1(Mo-S) + E(Mo-S) + 2A_1(Fe-S^b) + A_2(Fe-S^b) + 3E(Fe-S^b) \tag{3b}$$

A comparison of the Raman spectrum of **11** with that of the $MoFe_3S_4$−ethyl cluster **12** is given in Figure 8. Evidently, the spectrum of the $MoFe_3S_4$−ethyl cluster (upon which the structural model is based) and the spectrum of the $MoFe_3S_4$−benzyl cluster are quite similar, justifying the application of the structural model in Figure 7 to the $MoFe_3S_4$−benzyl cluster. The bands appearing at 470 cm^{-1} in the spectra of **11** and **12** are due to the ligands on the Mo center and/or the counterion; the band at 175 cm^{-1} may be an A_1(Fe/Mo) breathing vibration of the cluster primarily involving metal motion (cf. Table 3). The $Fe-S^{b/t}$ and $Mo-S^b$ stretching vibrations (eq 3a,b) thus appear in the range between 200 and 450 cm^{-1}. Because all modes with the exception of A_2 are IR and Raman active in C_{3v} symmetry, nine Mo/Fe−S vibrations are expected in this range. Moreover, in agreement with the higher charge of the cluster core and/or a greater Mo−S bond strength as compared to Fe−S, bands with a bridging S character in the $MoFe_3S_4$ spectra shift to higher energy with respect to the Fe_4S_4 clusters. This is particularly evident with respect to the highest energy bands of bridging character in the Fe_4S_4−benzyl cluster, III (T_2^b) and IV (A_1^b) (Figure 8). In contrast, band II (T_2^t) having predominantly terminal character remains almost stationary upon substitution of Fe by Mo. Further assignments were made on the basis of normal coordinate analysis (vide supra), performed with the program MOLVIB.[8] The Mo−O and Mo−S force constants were adjusted to optimally fit the observed frequencies. This way a force field was obtained which reproduced the observed frequencies quite well.

To check the corresponding band assignments, comparison with the spectra of corresponding halide clusters was employed. Infrared and Raman spectra of the Mo-substituted clusters $MoFe_3S_4Cl_4$ (**13**) and $MoFe_3S_4Br_4$ (**14**) are given along with those of their $Fe_4S_4Cl_4$ and $Fe_4S_4Br_4$ analogues **5** and **6** in Figures 9 and 10, respectively. Again, the bridging $T_2^b(T_d)$ modes III of the Fe_4S_4 units are easily recognized, shifting to higher energy in their respective $MoFe_3S_4$ counterparts. The terminal modes II (T_2^t), in contrast, almost remain at the same energy. The Raman intensities of the terminal modes are very low, which is similar to the case of the Fe_4S_4 clusters with terminal halide ligands. It is therefore justified to assign the intense band at 355 cm^{-1} in the Raman spectrum of $MoFe_3S_4$−benzyl cluster **11** (Figure 6), which is missing in the spectra of the halide coordinated clusters, to a terminal Fe−S stretching vibration (cf. Table 5). Furthermore, the terminal Mo−O stretching vibrations are located at about 520 cm^{-1} (Figure 6). Bridging modes of **11**, on the other hand, are located at 392 cm^{-1} (A_1^b, mainly Fe−S) and 415/427 cm^{-1} (A_1/E, mainly Mo−S), at which position they also appear in the $MoFe_3S_4$ halide coordinated clusters **13** and **14** (Figures 9 and 10).

Table 4. Geometry Parameters of $Fe_4(S/Se)_4$ Clusters with Terminal Halide Ligands

	compound	r^b	r^t	α	β	γ	b	a	c	ref	counterion in ref
5	$Fe_4S_4Cl_4$	2.283	2.217	103.5	74.6	114.9	2.766	3.587	3.793	9a	$(Et_4N)_2$-
6	$Fe_4S_4Br_4$	2.275	2.342	103.4	74.7	115.0	2.761	3.571	3.894	9b,c	$(PPh_4)_2$-
7	$Fe_4S_4I_4$	2.275	2.539	103.6	74.5	114.8	2.753	3.576	4.059	9d	$(PPh_4)_2$-
8	$Fe_4Se_4Cl_4$	2.400	2.215	105.6	71.8	113.1	2.813	3.823	3.852	9e	$(Et_4N)_2$-
9	$Fe_4Se_4Br_4$	2.403	2.359	105.9	71.4	112.9	2.803	3.836	3.968	9f	$(Et_4N)_2$-
10	$Fe_4Se_4I_4$	2.398	2.553	105.9	71.4	112.9	2.797	3.827	4.126	this paper	$(n\text{-}Bu_4N)_2$-

Table 5. Force Fields of the Halide Clusters (K^i, f_i, and F_i in mdyn·Å^{-1}; $r_i^2h_i$ in mdyn·Å)

K^b	K^t	f(b−t)	f(b−b)	$r_\alpha^2H_\alpha$	$r_\beta^2H_\beta$	$r_\gamma^2H_\gamma$	F_a (S^b−S^b)	F_b (Fe−Fe)	F_c (S^b−S^t)	a
					S−Cl (5)					
1.030	1.440	0	0.015	0	0	0.30	0.124	0.320	0.080	b
1.010	1.450	0.015	0	0	0	0.42	0.130	0.360	0.100	c
1.020	1.500	0	0	0	0	0.35	0.150	0.220	0.050	d
					S−Br (6)					
0.950	1.230	0.035	−0.010	0	0.12	0.45	0.120	0.400	0.100	
					S−I (7)					
0.900	1.220	0.080	0.025	0	0.20	0.55	0.110	0.320	0.090	c
0.910	1.220	0.080	0	0	0.20	0.55	0.160	0.180	0.065	d
					Se−I (8)					
0.830	0.980	0.025	0	0.05	0.10	0.32	0.080	0.320	0.100	
					Se−Br (9)					
0.915	1.080	0.055	−0.025	0	0.10	0.40	0.100	0.360	0.080	
					Se−Cl (10)					
0.925	1.380	0.055	−0.036	0	0	0.20	0.110	0.300	0.080	

[a] Alternate force fields.

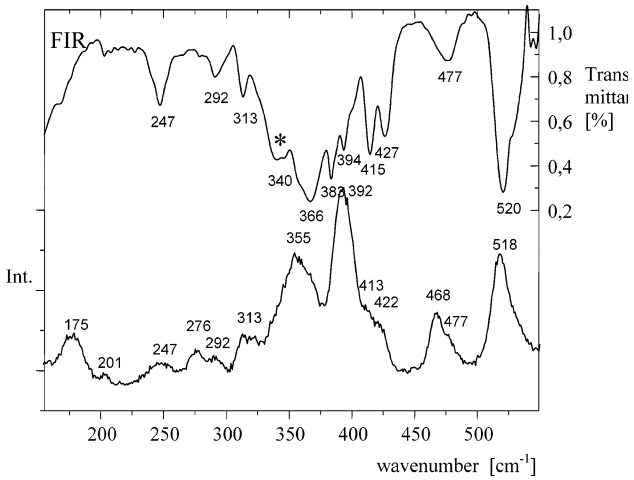

Figure 6. Raman and IR spectra of $[MoFe_3S_4(S-CH_2-Ph)_4]^{2-}$ (**11**). Asterisk (*) denotes δ(SCC) terminal ligand bend.

Calculated frequencies for $MoFe_3S_4$ cluster **11** are collected in Table 6 along with the observed values. Evidently, agreement between measured and calculated frequencies is excellent. The corresponding force constants evaluated in the Urey−Bradley force field (UBFF) are collected in Table 8. Remarkably, neither the terminal nor the bridging Fe−S force constants significantly differ from those of the Fe_4S_4 clusters, demonstrating the applicability of the force field of the benzyl cube.[3] The Mo−S force constant is evaluated to 2.1 mdyn/Å, about twice as large as the corresponding Fe−S force constant; the Mo−O force constant is found to be a similar value.

IV. Summary and Conclusions

In the present study, the vibrational structure of Mo/Fe−S/Se clusters with terminal thiolate and halide ligands has been investigated. The variety of compounds in conjunction with the available structural information allowed a systematic study of the spectroscopic properties of these systems. The missing member in the series of structurally characterized halide coordinated $Fe_4(S/Se)_4$ clusters, the iodo selenocluster $[Fe_4Se_4I_4]^{2-}$, has been subjected to an X-ray single-crystal structure determination. An important analytical tool in the spectroscopic investigation turned out to be the parallel analysis of IR and Raman spectra. In particular, the FTIR spectra allowed the unambiguous identification of T_2 modes.

In the accompanying paper, the stretching modes of the $Fe_4S^b{}_4$−methyl thiolate cluster have been assigned, starting from the force field of the benzyl cluster and considering the degrees of freedom of the terminal (t) thiolate ligands as

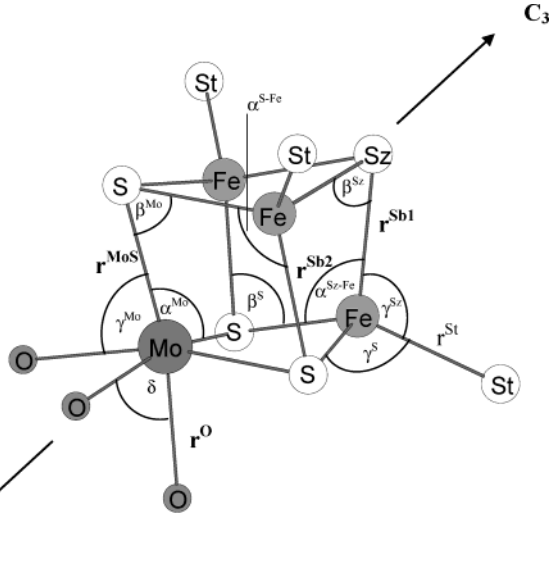

Figure 7. Structural model of the $MoFe_3S_4$ clusters with internal coordinate definitions.

Table 6. Fit to the Frequencies of $(NEt_4)_3[MoFe_3S_4(S-CH_2-C_6H_5)_3(Cl_4cat)CN]$ (**11**)

	Mo−O		Mo−S^b		Fe−S^b	Fe−S^t		Fe−S^b				
ν_s	A_1	E	E	A_1	A_1	E	A_1	E	E	A_2	A_1	E
obs	527	518	427	415	392	366	355	313	292		276	247
calcd	530	518	427	416	392	365	357	313	295	291	275	248

Table 7. Geometry Parameters of the $MoFe_3S_4$−Ethyl Cluster[a]

coordinate	r^{Sb1}	r^{Sb2}	r^{St}	r^{MoS}	r^O	α^{Mo}	α^{S-Fe}
$MoFe_3S_4(SEt)_3$	2.280	2.278	2.262	2.376	2.144	102.7	109.2
coordinate	α^{Sz-Fe}	β^{Mo}	β^S	β^{Sz}	γ^S	γ^{Sz}	γ^{Mo}
$MoFe_3S_4(SEt)_3$	104.1	72.1	72.9	72.8	112.9	112.9	87.5
coordinate	d	b^{Mo-Fe}	b^{Fe-Fe}	a^{S-S}	a^{S-Sz}	c^{St-S}	c^{St-Sz}
$MoFe_3S_4(SEt)_3$	79.8	2.741	2.707	3.712	3.594	3.784	3.785

[a] a, b, and c not shown in Figure 7.

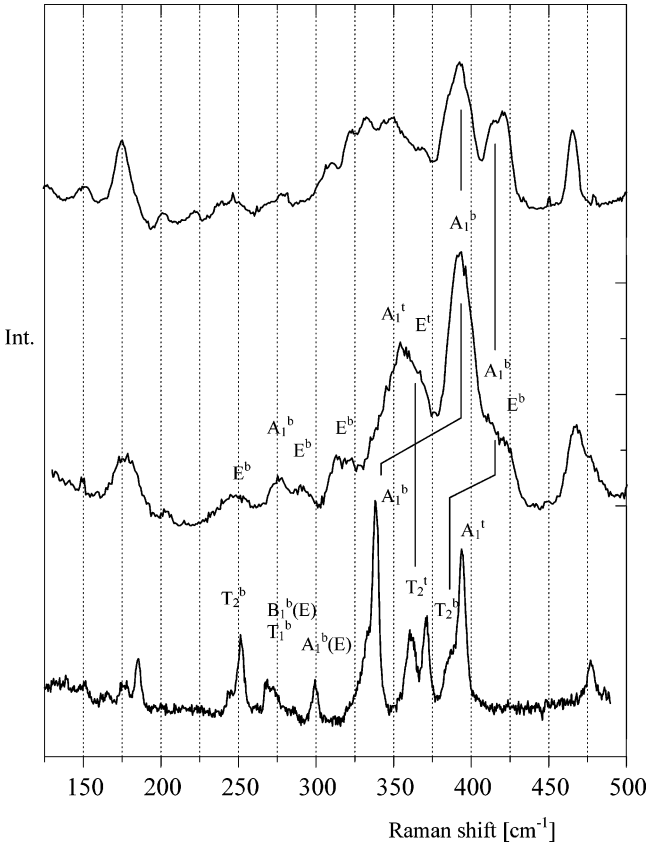

Figure 8. Raman spectra of the Fe_4S_4−benzyl cluster (BC, bottom; cf. accompanying paper), the $MoFe_3S_4$−benzyl cluster (**11**, middle), and the $MoFe_3S_4$−ethyl cluster (**12**, top), with band assignments.

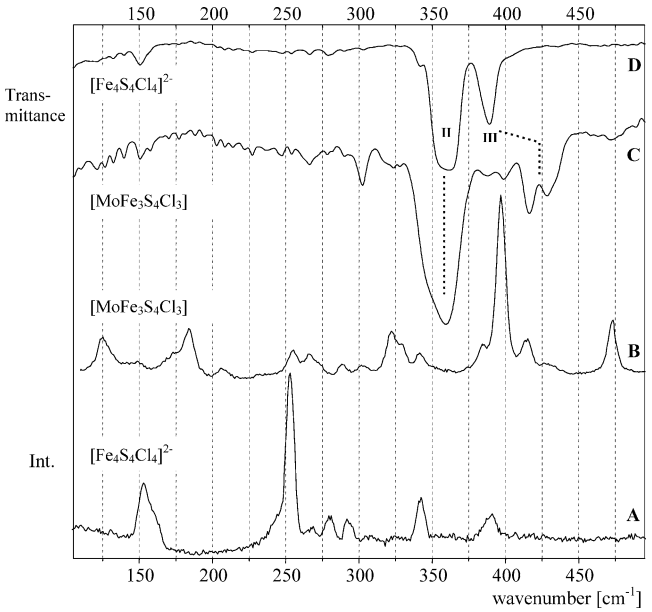

Figure 9. Raman (A, B) and IR (C, D) spectra of Fe_4S_4 and $MoFe_3S_4$ clusters with terminal halide ligands.

well. This force field was then used to account for the three other combinations S^b/Se^t, Se^b/S^t, and Se^b/Se^t. Remarkably, neither the $Fe-S^b/Fe-S^t$ valence force constants nor the Urey−Bradley nonbonding interactions were found to significantly change with respect to the parent $Fe_4S_4(S-CH_3)_4$ cluster. In the present paper, this analysis has been extended

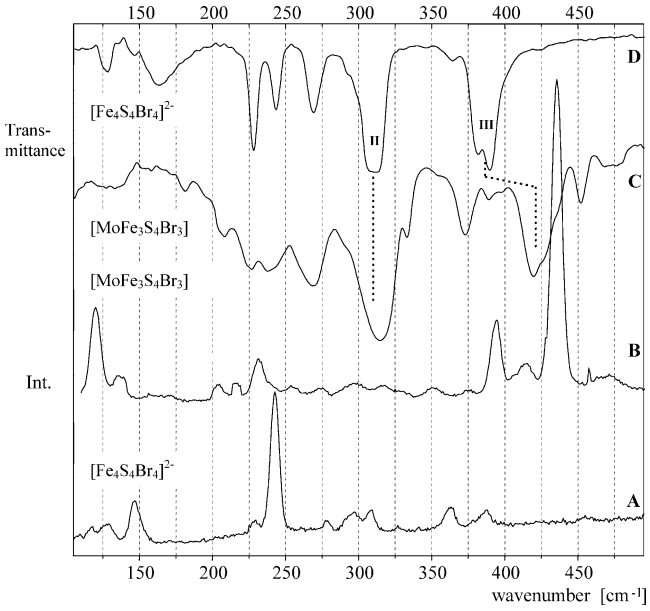

Figure 10. Raman (A, B) and IR (C, D) spectra of Fe_4S_4 and $MoFe_3S_4$ clusters with terminal bromo ligands.

Table 8. Urey−Bradley Force Constants for $[MoFe_3S^b_4(S^t)_3O_3]$, K_i, and F_i in mdyn/Å, and H_i in mdyn·Å[a]

force constant		description	force constant		description
K^{Sb1}	1.080	Fe−S3^b	$H_{\gamma\,Fe}$	0.42	S3^b-Fe−S^t
K^{Sb2}	1.080	Fe−S^b	H_{OO}	0.40	O−Mo−O
K^{MoS}	2.130	Mo−S	H_{OS}	0.48	O−Mo−S
K^t	1.365	Fe−S^t	F_{aFe}	0.080	S^b- - -S3^b
K^tO	2.060	Mo−O	F_{aMo}	0.080	S^b- - -S^b
$H_{\alpha Mo}$	0.0	S^b-Mo−S^b	F_{bFe}	0.240	Fe- - -Fe
$H_{\alpha Fe}$	0.0	S^b-Fe−S^b	F_{bMo}	0.300	Mo- - -Fe
$H_{\beta Mo}$	0.0	Mo−S^b-Fe	F_{cFe}	0.025	S3^b- - -S^t
$H_{\beta\,Fe}$	0.0	Fe−S^b-Fe	F_{cMo}	0.025	S^b- - -S^b
$H_{\gamma\,Mo}$	0.42	S^b-Fe−S^t			

[a] $H_{\alpha xy} = H_{\alpha z}$; $H_{\beta xy} = H_{\beta z}$; $H_{\gamma xy} = H_{\gamma z}$.

to $Fe_4(S/Se)_4$ clusters with terminal halide ligands, exploiting the spectral similarities between choro and thiolato coordinated clusters on one hand and bromo/selenolato coordinated clusters on the other hand. As expected from these analogies, the force field of the Fe_4S_4−benzyl cluster turned out to be applicable again.[3] To obtain optimal agreement between measured and calculated frequencies, however, additional small interaction constants had to be introduced in the analysis of the halide coordinated clusters which are not needed in the other systems.

The force field of the benzyl cube has finally been applied to Mo heterocubanes with terminal thiolate and halide ligands. As the substitution of an Fe by a Mo center entails significant changes in geometry and electronic structure, it had to be expected that the applicability of the force field of the benzyl cluster would eventually be limited. Nevertheless, for a first approximation of the $MoFe_3S_4$ force field, most force constants of the UBFF of the Fe_4S_4−benzyl cluster could be adopted. Only the Mo−O and Mo−S force constants had to be adjusted to match the corresponding frequencies. Further fitting did not lead to significant changes in the Fe−S force constants. The Mo−S valence force constant of 2.12 mdyn/Å was found to be about twice as

large as the Fe−S force constant, reflecting a greater Mo−S bond strength as compared to Fe−S. The Mo−O force constant accounting for an average interaction of the Mo center with the terminal ligands was found to be of similar magnitude.

In general, Raman intensities of the $MoFe_3S_4$ clusters were found to be weaker than those of their all-iron counterparts. This may in part be due to the shift of the bridging sulfur → metal CT transitions to the UV, thus decreasing resonance enhancement in the visible region. In addition, the line widths of the $MoFe_3S_4$ systems were found to be significantly larger than those exhibited by their all-iron counterparts, decreasing the *S*/*N* ratio and the resolution of the spectra. The reason for this finding may be the more complex and/or less symmetric coordination of the former systems, introducing additional vibrational couplings which act to broaden the bands. Nevertheless, for Mo-containing cubane clusters, Raman spectra of reasonable quality were obtained which could be correlated to those of their Fe_4S_4 counterparts.

To conclude, the force field of the Fe_4S_4−benzyl cluster has been found to be applicable to a wide range of cluster compounds derived from this system by substitution of the organic residues (benzyl → methyl, ethyl), the terminal donors (RS → RSe, Cl, Br, I), the bridging sulfur atoms (S → Se), and one of the iron atoms of the Fe_4S_4 unit (Fe → Mo), the last exchange being associated with a considerable change of the electronic structure of the cluster core. This provides an impressive demonstration of the generality of the employed UBFF originally developed for normal coordinate analysis of the benzyl cube, suggesting that it also may be applicable to more complicated iron−sulfur and heterometal/iron−sulfur clusters such as those existing in the MoFe protein of nitrogenase.

Acknowledgment. F.T. acknowledges funding of this research by the University of Kiel and the State of Schleswig-Holstein as well as FCI. A.K. acknowledges the help of Natascha Böres with the preparative work and of Uschi Cornelissen with the spectroscopic measurements.

Supporting Information Available: CIF file of the structure of **10**. This material is available free of charge via the Internet at http://pubs.acs.org.

IC030346L